Supplementary Information for "Enhanced Quantum Many-Body Scars in Non-Hermitian Systems"

Xinzhi Zhao[1,2], Wen-Yi Zhang[1,3], Ning Wu[4], Lin Zhuang[5], Wen-Long You[1,3,†], Xiangmei Duan[2,†], Wu-Ming Liu[6,†], and Chengjie Zhang[2,†]

[1] *College of Physics, Nanjing University of Aeronautics and Astronautics, Nanjing, 211106, China*

[2] *School of Physical Science and Technology, Ningbo University, Ningbo 315211, China*

[3] *Key Laboratory of Aerospace Information Materials and Physics (NUAA), MIIT, Nanjing, 211106, China*

[4] *Center for Quantum Technology Research, School of Physics, Beijing Institute of Technology, Beijing 100081, China*

[5] *School of Physics, Sun Yat-Sen University, Guangzhou 510275, China*

[6] *Institute of Physics, Chinese Academy of Sciences, Beijing 100190, China*

[†] E-mail: wlyou@nuaa.edu.cn; duanxiangmei@nbu.edu.cn; wmliu@iphy.ac.cn; zhangchengjie@nbu.edu.cn

CONTENTS

1. THEORETICAL METHODS

1.1. Mapping Kitaev model with uniaxial single-ion anisotropy onto the detuned PXP model

The Hamiltonian for the Kitaev model with uniaxial single-ion anisotropy reads

$$H_{\mathrm{KD}} = \sum_{j=1}^{L/2} \left[K(S^x_{2j-1}S^x_{2j} + S^x_{2j}S^y_{2j+1}) + D(S^z_j)^2 \right]. \tag{S1}$$

For convenience, we perform the unitary transformation on the even sites, i.e., $U = \prod_j \exp(i\pi S^x_{2j}) \exp\left(i\frac{\pi}{2}S^z_{2j}\right)$, and the rotated Hamiltonian becomes

$$\tilde{H}_{\mathrm{KD}} = U H_{\mathrm{KD}} U^\dagger = \sum_{j=1}^{L} \left[K S^x_j S^y_{j+1} + D(S^z_j)^2 \right]. \tag{S2}$$

Using the translation and $\mathbb{Z}_2$ symmetries of Eq. (S2), we can express its ground states on a two-site unit cell. For a pair of nearest neighbor sites $\langle j, j{+}1\rangle$, total $3{\times}3 = 9$ allowed states can be distinguished into the sector with positive gauge charge ($w_j = 1$) spanned by $|\bullet\bullet\rangle$, $|\bullet\bullet\rangle$, $|\bullet\bullet\rangle$, $|\bullet\bullet\rangle$, $|\bullet\bullet\rangle$ and the $w_j = -1$ sector spanned by $|\bullet\bullet\rangle$, $|\bullet\bullet\rangle$, $|\bullet\bullet\rangle$, $|\bullet\bullet\rangle$.

The one-to-one mapping between the 5 allowed two-site configurations for a pair of nearest neighbor sites $\langle j, j{+}1\rangle$ and spin-1/2 degree of freedom for the bond center $j + 1/2$ is given by

$$\begin{aligned}
&|\cdots\bullet\bullet\cdots\rangle_{j,j+1} \leftrightarrow |\cdots\downarrow\cdots\rangle_{j+\frac{1}{2}},\\
&|\cdots\bullet\bullet\cdots\rangle_{j,j+1} \leftrightarrow |\cdots\uparrow\cdots\rangle_{j+\frac{1}{2}},\\
&|\cdots\bullet\bullet\cdots\rangle_{j,j+1} \leftrightarrow |\cdots\downarrow\cdots\rangle_{j+\frac{1}{2}},\\
&|\cdots\bullet\bullet\cdots\rangle_{j,j+1} \leftrightarrow |\cdots\downarrow\cdots\rangle_{j+\frac{1}{2}},\\
&|\cdots\bullet\bullet\cdots\rangle_{j,j+1} \leftrightarrow |\cdots\downarrow\cdots\rangle_{j+\frac{1}{2}},.
\end{aligned} \tag{S3}$$

It is worthy noting that the prime lattice of the spin-1 Kitaev chain is defined on the sites $\{j\}$, while the dual lattice of spin-1/2 PXP model lives on the linking bonds at sites $\{j{+}1/2\}$. Although the mapping seems to be many to one at first glance, it is in fact invertible. The mapping from the dual lattice back to the spin-1 lattice reads

$$\begin{aligned}
&|\cdots\downarrow\uparrow\cdots\rangle_{j-\frac{1}{2},j+\frac{1}{2}} \to |\cdots\bullet\cdots\rangle_j\\
&|\cdots\uparrow\downarrow\cdots\rangle_{j-\frac{1}{2},j+\frac{1}{2}} \to |\cdots\bullet\cdots\rangle_j\\
&|\cdots\downarrow\downarrow\cdots\rangle_{j-\frac{1}{2},j+\frac{1}{2}} \to |\cdots\bullet\cdots\rangle_j.
\end{aligned} \tag{S4}$$

In this case, Eqs. (S3) and (S4) ensure that the mapping is one to one for periodic boundary conditions.

The local two-spin Hamiltonian is given by

$$\tilde{H}_{j,j+1} = K S_j^x S_{j+1}^y + D[(S_j^z)^2 + (S_{j+1}^z)^2]. \tag{S5}$$

For the 5 states satisfying $w_j = 1$, we have

$$\begin{aligned}
&\tilde{H}_{j,j+1}|\bullet\bullet\rangle = 2D|\bullet\bullet\rangle, \quad \tilde{H}_{j,j+1}|\bullet\bullet\rangle = D|\bullet\bullet\rangle,\\
&\tilde{H}_{j,j+1}|\bullet\bullet\rangle = D|\bullet\bullet\rangle, \quad \tilde{H}_{j,j+1}|\bullet\bullet\rangle = K|\bullet\bullet\rangle,\\
&\tilde{H}_{j,j+1}|\bullet\bullet\rangle = K|\bullet\bullet\rangle + 2D|\bullet\bullet\rangle.
\end{aligned} \tag{S6}$$

Accordingly, the Hamiltonian can be written in the matrix form as

$$\tilde{H}_{j,j+1} = \begin{pmatrix} 2D & 0 & 0 & 0 & 0 \\ 0 & D & 0 & 0 & 0 \\ 0 & 0 & D & 0 & 0 \\ 0 & 0 & 0 & 2D & K \\ 0 & 0 & 0 & K & 0 \end{pmatrix}, \tag{S7}$$

which yields 5 energy eigenvalues $2D$,D,D,$D \pm \sqrt{D^2 + K^2}$. Hence, within the lowest-state manifold residing in the $w_j = 1$ sector that is spanned by $\{|\bullet\bullet\rangle, |\bullet\bullet\rangle\}$. The process of bond converting $|\cdots\bullet\bullet\cdots\rangle_{j,j+1} \leftrightarrow |\cdots\bullet\bullet\cdots\rangle_{j,j+1}$ under the action of $\tilde{H}_{\rm K}$ corresponds to the spin flip $|\cdots\downarrow\cdots\rangle_{j+1/2} \leftrightarrow |\cdots\uparrow\cdots\rangle_{j+1/2}$ in $\{\mathcal{K}_{S=1/2}\}$ under the action of $H_{\rm PXP}$. In this regard, the spin-1 Kitaev chain with periodic boundary conditions can be exactly mapped to the a single qubit-flip model represented by the effective spin-1/2 PXP model. Remarkably, we find the ground state remains in the flux-free sector even in the presence of the uniaxial SIA. The action of the uniaxial SIA term on the active bases yields,

$$\begin{aligned}
&D\left[(S_j^z)^2 + (S_{j+1}^z)^2\right]|\cdots\bullet\bullet\cdots\rangle_{j,j+1} = 2D|\cdots\bullet\bullet\cdots\rangle_{j,j+1},\\
&D\left[(S_j^z)^2 + (S_{j+1}^z)^2\right]|\cdots\bullet\bullet\cdots\rangle_{j,j+1} = 0,
\end{aligned} \tag{S8}$$

which results in an effective detuning term on the spin-1/2 degrees of freedom, i. e.,

$$\begin{aligned}
&2D \cdot n_{j+1/2}|\cdots\uparrow\cdots\rangle_{j+1/2} = 2D|\cdots\uparrow\cdots\rangle_{j+1/2},\\
&2D \cdot n_{j+1/2}|\cdots\downarrow\cdots\rangle_{j+1/2} = 0.
\end{aligned} \tag{S9}$$

Therefore, the spin-1 Kitaev chain with uniaxial SIA can be mapped to the spin-1/2 detuned PXP model,

$$\hat{H}_{\rm dPXP} = K\sum_{i=1}^{N} P_{i-1}X_iP_{i+1} + 2D\sum_{i=1}^{N} P_{i-1}n_iP_{i+1}, \tag{S10}$$

where $n = 1 - P = |\uparrow\rangle\langle\uparrow|$ and X_i is the Pauli-X matrix.

1.2. The detuned PXP Model

Consider the detuned PXP model in Eq.(S10) with $L = 6$ sites with $K = 1$,

$$H_{\rm dPXP} = H_{\rm PXP} + H_{\rm PNP},$$

where

$$\begin{aligned} H_{\rm PXP} &= \sum_{i=1}^{6} P_{i-1}\sigma_i^x P_{i+1}, \\ H_{\rm PNP} &= 2D\sum_{i=1}^{6} P_{i-1}n_i P_{i+1}, \end{aligned} \tag{S11}$$

where $P_i = (1-\sigma_i^z)/2$ and $n_i = (1+\sigma_i^z)/2$. We impose the periodic boundary conditions, i.e., $\sigma_{L+1}^{\alpha} = \sigma_1^{\alpha}$. The PXP part $H_{\rm PXP}$ does not conserve the total magnetization M_z along the z-axis and change M_z by one unit, so that it anticommutes with the parity operator of the number of down spins, $\mathcal{P} = \prod_{i=1}^{6}\sigma_i^z$. As a result, for $D = 0$ the spectrum is symmetric with respect to the zero energy: $H_{\rm PXP}(\mathcal{P}|E\rangle) = -\mathcal{P}H_{\rm PXP}|E\rangle = -E(\mathcal{P}|E\rangle)$.

We take the fully polarized state $|F\rangle = |\downarrow\downarrow\downarrow\downarrow\downarrow\downarrow\rangle$ as a reference state. To construct all the Bloch states for a six-site PXP-PNP ring, we use the following mapping between basis states of the spin-1 Kitaev model and the PXP model

$$|\bullet\bullet\bullet\bullet\bullet\bullet\rangle \leftrightarrow |\uparrow\downarrow\downarrow\uparrow\downarrow\downarrow\rangle. \tag{S12}$$

Note that there is always an '$\bullet$' ('$\downarrow$') on the right of '$\bullet$' ('$\uparrow$').

1.3. The non-Hermitian PXP Model

We consider the operator $X_i = |\downarrow\rangle_i\langle\uparrow|_i + |\uparrow\rangle_i\langle\downarrow|_i$. To introduce non-Hermiticity, the symmetric coupling between $|\uparrow\rangle$ and $|\downarrow\rangle$ is generalized to a non-reciprocal form, expressed

as

$$|\downarrow\rangle_i\langle\uparrow|_i + |\uparrow\rangle_i\langle\downarrow|_i \rightarrow (1-g)\ |\downarrow\rangle_i\langle\uparrow|_i + (1+g)\ |\uparrow\rangle_i\langle\downarrow|_i, \tag{S13}$$

resulting in a non-Hermitian PXP Hamiltonian given by

$$\hat{H}_{\mathrm{nH-dPXP}} = \sum_{i=1}^{N} P_{i-1}(X_i + igY_i)P_{i+1} + 2D\sum_{i=1}^{N} P_{i-1}n_iP_{i+1}, \tag{S14}$$

where the parameter g quantifies the strength of non-Hermiticity, and Y_i is the Pauli-Y matrix.

1.4. Complete set of Bloch states

Beside the reference state $|F\rangle = |\downarrow\downarrow\downarrow\downarrow\downarrow\downarrow\rangle$, we construct the remaining 17 Bloch states as follows:

i) One-magnon Bloch states.

$$|\psi(k \in K_0)\rangle = \frac{1}{\sqrt{6}}\sum_{n=0}^{5} e^{ikn}T^n|\bullet\bullet\bullet\bullet\bullet\bullet\rangle, \tag{S15}$$

where T is the translation operator by one lattice spacing. The wave number k takes values in the set ($e^{i6k} = 1$)

$$K_0 = \left\{-\pi, -\frac{2}{3}\pi, -\frac{\pi}{3}, 0, \frac{\pi}{3}, \frac{2}{3}\pi\right\} \tag{S16}$$

to ensure the translational invariance of $|\psi(k)\rangle$, i.e., $T|\psi(k)\rangle = e^{-ik}|\psi(k)\rangle$. There are totally 6 one-magnon Bloch states.

ii) Two-magnon Bloch states.

$$|\psi_2(k \in K_0)\rangle = \frac{e^{ik}}{\sqrt{N}}\sum_{n=0}^{5} e^{ikn}T^n|\bullet\bullet\bullet\bullet\bullet\bullet\rangle, \tag{S17}$$

and

$$|\psi_3(k \in K_1)\rangle = \frac{e^{i\frac{3}{2}k}}{\sqrt{3}}\sum_{n=0}^{2} e^{ikn}T^n|\bullet\bullet\bullet\bullet\bullet\bullet\rangle. \tag{S18}$$

In the above expressions, the subscript in each state indicates the separation between the two excitations. Note that the k in $|\psi_3(k)\rangle$ is restricted to the following subset of K_0 ($e^{i3k} = 1$):

$$K_1 = \left\{-\frac{2\pi}{3}, 0, \frac{2\pi}{3}\right\}. \tag{S19}$$

Thus, there are totally $6+3=9$ two-magnon Bloch states.

iii) Three-magnon Bloch states.

$$|\psi_{2,2}(k\in K_2)\rangle = \frac{e^{i2k}}{\sqrt{2}}\sum_{n=0}^{1} e^{ikn}T^n|\bullet\bullet\bullet\bullet\bullet\bullet\rangle, \tag{S20}$$

Similarly, the two indices denote the two separations between the three local excitations. The k in $|\psi_{2,2}(k)\rangle$ takes values in the subset

$$K_2 = \{-\pi, 0\}\,. \tag{S21}$$

There are totally 2 three-magnon Bloch states.

After a straightforward calculation, we find that for each fixed k the allowed Bloch states form a closed set under the action of the Hamiltonian, resulting in four different types of effective single-particle Hamiltonians with dimensions given by

$$\begin{aligned}
&5,\ k=0,\ \{|F\rangle, |\psi(0)\rangle, |\psi_2(0)\rangle, |\psi_3(0)\rangle, |\psi_{2,2}(0)\},\\
&3,\ k=-\pi,\ \{|\psi(-\pi)\rangle, |\psi_2(-\pi)\rangle, |\psi_{2,2}(-\pi)\rangle\},\\
&6=3\times 2,\ k=\pm\frac{2}{3}\pi,\ \{|\psi(\pm\frac{2}{3}\pi)\rangle, |\psi_2(\pm\frac{2}{3}\pi)\rangle, |\psi_3(\pm\frac{2}{3}\pi)\rangle\},\\
&4=2\times 2,\ k=\pm\frac{\pi}{3},\ \{|\psi(\pm\frac{\pi}{3})\rangle, |\psi_2(\pm\frac{\pi}{3})\rangle\}.
\end{aligned} \tag{S22}$$

1.5. Non-Hermitian PXP Hamiltonian in the subspace of $k=-\pi$

We now focus on the $k=-\pi$ subspace. Direct calculation gives

$$H_{\mathrm{PXP}}^{(-\pi)} = \begin{pmatrix} 0 & -2 & 0\\ -2 & 0 & -\sqrt{3}\\ 0 & -\sqrt{3} & 0 \end{pmatrix}, \tag{S23}$$

in the basis $\{|\psi(-\pi)\rangle, |\psi_2(-\pi)\rangle, |\psi_{2,2}(-\pi)\rangle\}$.

It is obvious that

$$H_{\mathrm{PNP}}^{(-\pi)} = \begin{pmatrix} 2D & 0 & 0\\ 0 & 4D & 0\\ 0 & 0 & 6D \end{pmatrix}. \tag{S24}$$

Hence,

$$H_{\mathrm{dPXP}}^{(-\pi)} = \begin{pmatrix} 2D & -2 & 0 \\ -2 & 4D & -\sqrt{3} \\ 0 & -\sqrt{3} & 6D \end{pmatrix}. \tag{S25}$$

For completeness, we also write down $H_{\mathrm{dPXP}}^{(0)}$ in the basis $\{|F\rangle, |\psi(0)\rangle, |\psi_2(0)\rangle, |\psi_3(0)\rangle, |\psi_{2,2}(0)\}$:

$$H_{\mathrm{dPXP}}^{(0)} = \begin{pmatrix} 0 & \sqrt{6} & 0 & 0 & 0 \\ \sqrt{6} & 2D & 2 & \sqrt{2} & 0 \\ 0 & 2 & 4D & 0 & \sqrt{3} \\ 0 & \sqrt{2} & 0 & 4D & 0 \\ 0 & 0 & \sqrt{3} & 0 & 6D \end{pmatrix}, \tag{S26}$$

for comparison with exact diagonalization. The non-Hermitian Hamiltonian can be written as

$$H_{\mathrm{nH-dPXP}}^{(-\pi)} = \begin{pmatrix} 2D & -2(1-g) & 0 \\ -2(1+g) & 4D & -\sqrt{3}(1-g) \\ 0 & -\sqrt{3}(1+g) & 6D \end{pmatrix}. \tag{S27}$$

1.6. Varying system sizes

To further substantiate the generality of our theoretical model, we have extended our analysis to systems with varying of system sizes. This section presents complementary theoretical results that demonstrate the existence of perfect QMBS in these extended parameter spaces (see Fig. S1). We have numerically verified that the high-fidelity of perfect scars emerge consistently across different system sizes. This includes one-dimensional chains with increased system sizes. Across the full space, we notice a clear pattern: the closer the parameter g is to an exceptional point (EP, $|g| = 1$), the more easily perfect scars appear. This proximity dependence appears insensitive to the actual system size. It's as if the EP acts like a focal point, pulling the dynamics toward states that can sustain these exact scars.

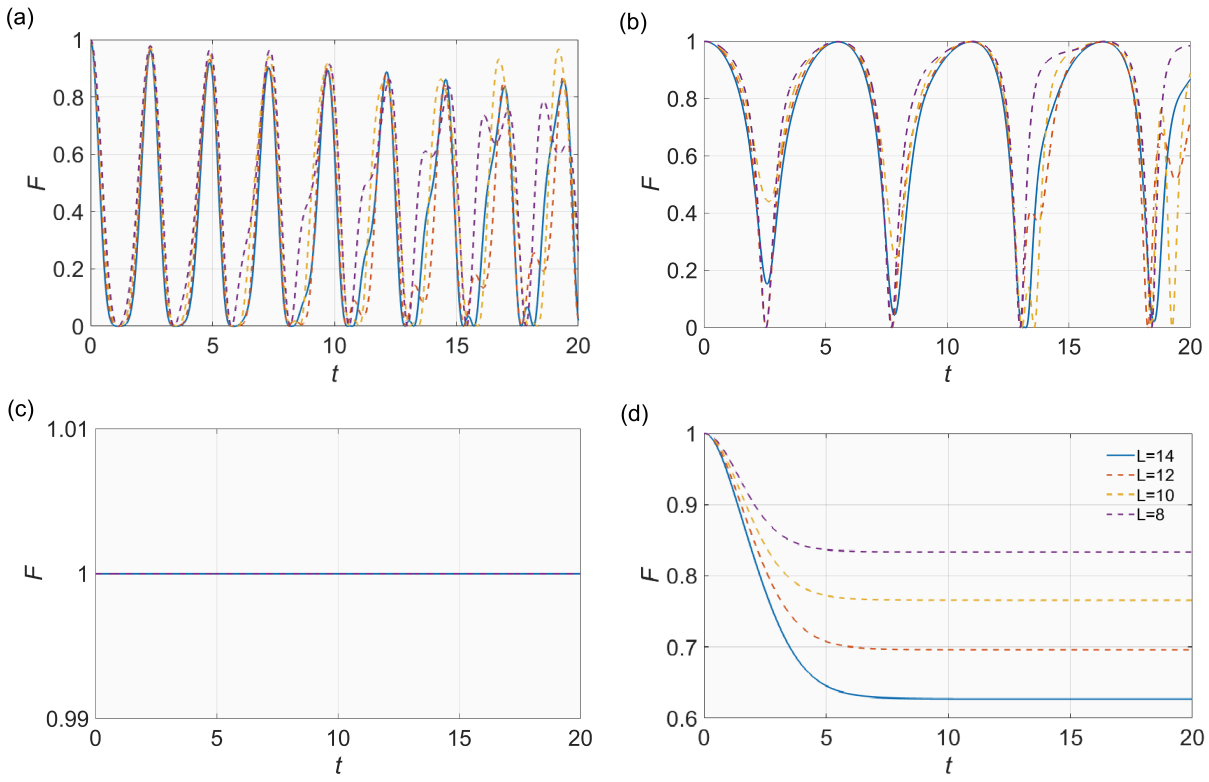

Figure S1. Time evolution of the normalized fidelity (F) for different system sizes, (a) $g = 0.2$, (b) $g = 0.9$, (c) $g = 1.0$, (d) $g = 1.1$. With increasing system size, With increasing system size, the high-fidelity plateaus shrink toward the exceptional point at $g = 1$, indicating that scarred oscillations induced by the non-Hermitian term persist across lattice sizes.

2. THE SCHEME OF THE EXPERIMENT

Before delving into the specifics of our experimental procedure, we will first introduce the critical components within the optical components:

1). According to our experimental requirements, we have definedthe horizontal polarization state $|\mathrm{H}\rangle$ and the vertical polarization state $|\mathrm{V}\rangle$ as follows

$$|\mathrm{H}\rangle := |0\rangle = \begin{pmatrix} 1 \\ 0 \end{pmatrix}, |\mathrm{V}\rangle := |1\rangle = \begin{pmatrix} 0 \\ 1 \end{pmatrix}. \tag{S28}$$

2). The beam displacer (BD) is capable of fully transmitting horizontally polarized photons, but diverting them from their original path when they emit vertically polarized photons (4 mm in our experiments).

3). Polarization beam splitter (PBS) can divide polarized light into two paths, namely horizontal polarized light transmission and vertical polarized light reflection.

4). Dichroic mirror (DM) reflects light at a wavelength of 405 nm while allowing light at 810 nm to transmit.

5). We use half-wave plates (HWP: α) and quarter-wave plates (QWP: β) to implement unitary operation. The α or β here refers to the angle between the fast axis of the waveplate and the horizontal polarization direction. The *Jones matrix* of waveplates can be denoted as [1]

$$\mathrm{HWP}(\alpha) = \begin{pmatrix} \cos 2\alpha & \sin 2\alpha \\ \sin 2\alpha & -\cos 2\alpha \end{pmatrix}, \mathrm{QWP}(\beta) = \begin{pmatrix} \cos^2\beta + i\sin^2\beta & (1-i)\cos\beta\sin\beta \\ (1-i)\cos\beta\sin\beta & \sin^2\beta + i\cos^2\beta \end{pmatrix}. \tag{S29}$$

2.1. The heralded single-photon source

The experimental procedure necessitates a pump light, which is produced by an ultraviolet laser diode (LD) that has a central wavelength set at 405 nm. As shown in Fig.S2, the power of the pump light can be adjusted by the wave plate group (HWP and QWP) and PBS (see section of I). Then PBS and HWP are used to prepare the polarization state of the pump light (see section II). Here, the HWP is rotated by 0° (the angle between the fast axis and the horizontal direction). The crystal is operated at a temperature of 25°C.

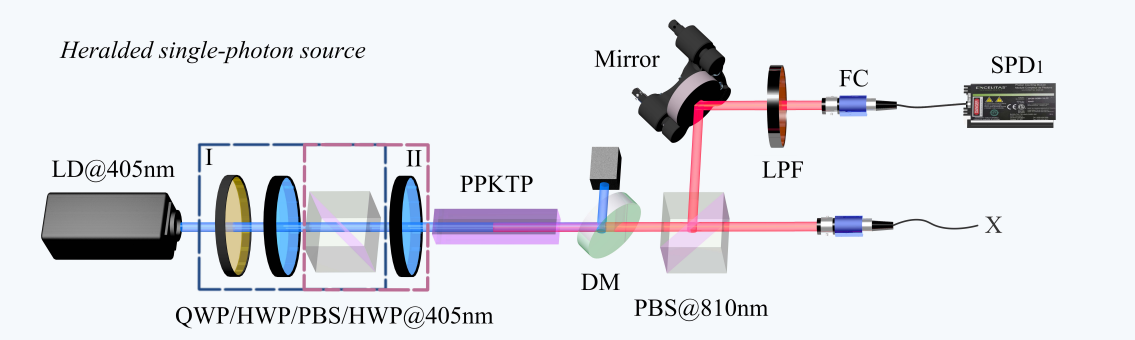

Figure S2. Experimental setup of the heralded single-photon source. (I)The 405 nm continuous-wave laser (LD@405 nm) passes through an isolator followed by a quarter-wave plate (QWP@405 nm), half-wave plate (HWP@405 nm) and polarizing beam splitter (PBS@405 nm) for power control. (II) After a PBS, the HWP (405 nm) polarization pure module the beam is focused into a PPKTP crystal (type-II SPDC). Signal and idler photons are separated from the pump by a dichroic mirror (DM) and a long-pass filter (LPF), then collected by a single-mode fiber coupler (FC). The idler photons are routed to a single photon detector (SPD). The single photons are collected by the X port and then transmitted to the subsequent experimental setup paths.

Because of the small size of the PPKTP crystal, two lenses are used to focus and reduce the diameter of the pump light (we do not include these in Fig. S2, the two lenses are matched to a wavelength of $405nm$). The generation of photon pairs at 810 nm is achieved through type-II spontaneous parametric down-conversion (SPDC). In type-II SPDC, there indeed exists a specific polarization configuration where the signal photon and the idler photon are produced with orthogonal polarization states. This occurs because, within a nonlinear crystal, the pump photon can generate two photons with different polarization directions through nonlinear interaction. Specifically, if the pump photon is linearly polarized, for instance, horizontally polarized ($|H_{\text{pump}}\rangle$), then through the process of type-II SPDC, a pair of photons can be produced where one is vertically polarized ($|V_{\text{signal}}\rangle$ or $|V_{\text{idel}}\rangle$) and the other remains horizontally polarized ($|H_{\text{signal}}\rangle$ or $|H_{\text{idel}}\rangle$), or vice versa. Since the DM reflects the 405 nm pump light, the generated photon pairs at 810 nm naturally separate into two paths after passing through the PBS. Among them, the idler photon pairs, after passing through a long-pass filter (LPF) and being coupled by a fiber coupler (FC), are collected using a single-photon detector (SPD_1). The signal photons are coupled via FC and fed into the experimental optical path at port X (see Fig. S2) through a single-mode fiber.

Ultimately within the experimental optical path, the signal photons are collected by $\mathrm{SPD}_{2,3}$, and coincidence counting is performed between SPD_1 and $\mathrm{SPD}_{2,3}$.

The construction method for a heralded single-photon source is not limited to the type illustrated in Fig. S2; if necessary, references to other types of articles may also be consulted [2–6].

2.2. Evolution method for Hermitian Hamiltonian $g = 0$

In this experiment, we have realized the Hermitian Hamiltonian $H = H_{\mathrm{dPXP}}^{(-\pi)}$, the expression of which is presented in Eq. (S25). Under the context of 3d space, we have adopted a method that decomposes unitary operations into a product of a series of 2d unitary matrices [7]. Specifically, this decomposition is represented in the form of $U = U_{13}U_{23}U_{12}$, where $U = e^{-iHt}$ denotes the overall unitary operation, and U_{ij} $(i, j = 1, 2, 3)$ represents the individual 2d unitary matrices that constitute U. The experimental setup of the evolution method for Hermitian model is shown in Fig. S3. The initial state prepared in the experiment as $|\psi_3(\pi)\rangle = (|\mathbb{Z}_2\rangle - |\mathbb{Z}_2'\rangle)/\sqrt{2}$ with $L = 6$, which is represented by $|3\rangle := |\mathrm{H}\rangle|\mathrm{down}_1\rangle$, where $|\mathrm{H}\rangle$ represent the horizontal polarization information. $|\mathrm{up_m}\rangle$ and $|\mathrm{down_m}\rangle$ $(\mathrm{m} = 1, 2, 3, 4)$ denote the path information after BD, respectively.

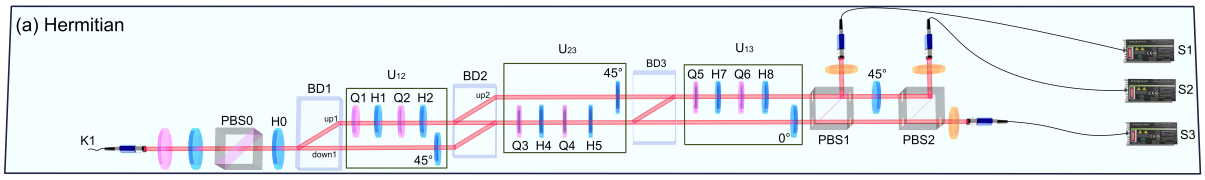

Figure S3. Experimental setup of the Hermitian model. We use PBS_0, H_1 and BD_1 to encode the polarization information of the signal photons entering at port K_1 and to prepare the required initial state. The additional HWP at 45° on the $|\mathrm{down}_1\rangle$ path flips polarisation so that this beam is steered upward by BD_2. After BD_2 with a 45° HWP on $|\mathrm{up}_2\rangle$ that closes the interference network.

In the following, we denote α_k as the angle of the half wave plate H_k (with k form 0 to 17), and denote β_t as the angle of the quarter wave plate Q_t (with t from 1 to 10).

2.2.1. *Evolution under parameter $D = 0$*

According to the Eq. (S25), the Hamiltonian H_0 with $D = 0$ can be expressed as

$$H_0 = \begin{pmatrix} 0 & -2 & 0 \\ -2 & 0 & -\sqrt{3} \\ 0 & -\sqrt{3} & 0 \end{pmatrix}. \tag{S30}$$

Since its evolved form is $U_0 = e^{-iH_0 t}$, its matrix representation can be formulated as

$$U_0 = \begin{pmatrix} \frac{1}{7}(3 + 4\cos\sqrt{7}t) & \frac{2i\sin\sqrt{7}t}{\sqrt{7}} & \frac{2\sqrt{3}}{7}(-1 + \cos\sqrt{7}t) \\ \frac{2i\sin\sqrt{7}t}{\sqrt{7}} & \cos\sqrt{7}t & -i\sqrt{\frac{3}{7}}\sin\sqrt{7}t \\ \frac{2\sqrt{3}}{7}(-1 + \cos\sqrt{7}t) & -i\sqrt{\frac{3}{7}}\sin\sqrt{7}t & \frac{1}{7}(3 + 4\cos\sqrt{7}t) \end{pmatrix}. \tag{S31}$$

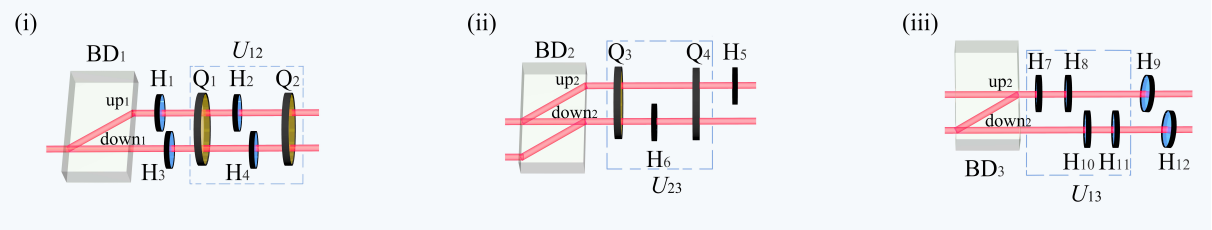

Figure S4. Experimental setup of $D = 0$. The core principle involves decomposing the target quantum operator into a series of elementary unitary operators U_{ij}, which are physically realized via path encoding. Waveplates (H_{1-12} and Q_{1-4}) set at specific angles perform the corresponding unitary operations. The initial state evolves through conditional operations applied along these paths, and finally outputs the target quantum state via path merging and interference. Detailed configurations of optical components and their corresponding state evolution results are provided in the Table. I.

The experimental setup of unitary operator $U_0 = U_{13}U_{23}U_{12}$ is shown in Fig. S4. The decomposed U_{12}, U_{23} and U_{13} takes the following theoretical for as

$$U_{12} = \begin{pmatrix} \frac{\sqrt{7}\cos\sqrt{7}t}{(4+3\cos\sqrt{7}t)\sqrt{\frac{4+3\cos^2\sqrt{7}t}{(4+3\cos\sqrt{7}t)^2}}} & \frac{2i\sin\sqrt{7}t}{(4+3\cos\sqrt{7}t)\sqrt{\frac{4+3\cos^2\sqrt{7}t}{(4+3\cos\sqrt{7}t)^2}}} & 0 \\ \frac{2i\sin\sqrt{7}t}{(4+3\cos\sqrt{7}t)\sqrt{\frac{4+3\cos^2\sqrt{7}t}{(4+3\cos\sqrt{7}t)^2}}} & \frac{\sqrt{7}\cos\sqrt{7}t}{(4+3\cos\sqrt{7}t)\sqrt{\frac{4+3\cos^2\sqrt{7}t}{(4+3\cos\sqrt{7}t)^2}}} & 0 \\ 0 & 0 & 1 \end{pmatrix}, \tag{S32}$$

$$U_{23} = \begin{pmatrix} 1 & 0 & 0 \\ 0 & \frac{11+3\cos 2\sqrt{7}t}{2\sqrt{7}(4+3\cos\sqrt{7}t)\sqrt{\frac{4+3\cos^2\sqrt{7}t}{(4+3\cos\sqrt{7}t)^2}}} & i\sqrt{\frac{3}{7}}\sin\sqrt{7}t \\ 0 & i\sqrt{\frac{3}{7}}\sin\sqrt{7}t & \frac{11+3\cos 2\sqrt{7}t}{2\sqrt{7}(4+3\cos\sqrt{7}t)\sqrt{\frac{4+3\cos^2\sqrt{7}t}{(4+3\cos\sqrt{7}t)^2}}} \end{pmatrix}, \tag{S33}$$

$$U_{13} = \begin{pmatrix} \frac{1}{\sqrt{7}\sqrt{\frac{4+3\cos^2\sqrt{7}t}{(4+3\cos\sqrt{7}t)^2}}} & 0 & \frac{2\sqrt{\frac{6}{7}}(-1+\cos\sqrt{7}t)}{(4+3\cos\sqrt{7}t)\sqrt{\frac{11+3\cos 2\sqrt{7}t}{(4+3\cos\sqrt{7}t)^2}}} \\ 0 & 1 & 0 \\ \frac{2\sqrt{\frac{6}{7}}(1-\cos\sqrt{7}t)}{(4+3\cos\sqrt{7}t)\sqrt{\frac{11+3\cos 2\sqrt{7}t}{(4+3\cos\sqrt{7}t)^2}}} & 0 & \frac{1}{\sqrt{7}\sqrt{\frac{4+3\cos^2\sqrt{7}t}{(4+3\cos\sqrt{7}t)^2}}} \end{pmatrix}. \tag{S34}$$

In the experiment, we selected $|\psi_0\rangle = |3\rangle := |\mathrm{H}\rangle|\mathrm{down}_1\rangle$ as the initial state. The state evolved from the initial state by U_0 is recorded in Table. I for reference. Since we employed a method with a fixed initial state, the corresponding experimental outcomes were obtained by adjusting the evolution parameter t, with different values of t being achieved by altering the angles of the HWPs in each U_{ij}.

TABLE I. The preparation of the unitary operators U_0 in the case of $D = 0$.

State prepared	Result
H_0 ($\alpha_0 = 0°$)	$\|0\rangle$
BD_1	$\|0\rangle\|\mathrm{down}_1\rangle$
H_3 ($\alpha_3 = 45°$)	$\|1\rangle\|\mathrm{down}_1\rangle$
Q_1 ($\beta_1 = 0°$)	$i\|1\rangle\|\mathrm{down}_1\rangle$
H_4 ($\alpha_4 = 0°$)	$-i\|1\rangle\|\mathrm{down}_1\rangle$
Q_2 ($\beta_2 = 0°$)	$\|1\rangle\|\mathrm{down}_1\rangle$
BD_2	$\|1\rangle\|\mathrm{dowm}_2\rangle$
Q_3 ($\beta_3 = 0°$)	$i\|1\rangle\|\mathrm{down}_2\rangle$
H_6 (α_6)	$i\sin 2\alpha_6\|0\rangle\|\mathrm{down}_2\rangle - \mathrm{i}\cos 2\alpha_6\|1\rangle\|\mathrm{down}_2\rangle$
Q_4 ($\beta_4 = 0°$)	$i\sin 2\alpha_6\|0\rangle\|\mathrm{down}_2\rangle + \cos 2\alpha_6\|1\rangle\|\mathrm{down}_2\rangle$
BD_3	$i\sin 2\alpha_6\|0\rangle\|\mathrm{down}_2\rangle + \cos 2\alpha_6\|1\rangle\|\mathrm{up}_2\rangle$
H_7 (α_7)	$i\sin 2\alpha_6\|0\rangle\|\mathrm{down}_2\rangle + (\cos 2\alpha_6 \sin 2\alpha_7\|0\rangle - \cos 2\alpha_6 \cos 2\alpha_7\|1\rangle)\|\mathrm{up}_2\rangle$
H_8 ($\alpha_8) = 0°$	$i\sin 2\alpha_6\|0\rangle\|\mathrm{down}_2\rangle + (\cos 2\alpha_6 \sin 2\alpha_7\|0\rangle + \cos 2\alpha_6 \cos 2\alpha_7\|1\rangle)\|\mathrm{up}_2\rangle$
H_{10-11} ($\alpha_{10-11}) = 0°$	$i\sin 2\alpha_6\|0\rangle\|\mathrm{down}_2\rangle + (\cos 2\alpha_6 \sin 2\alpha_7\|0\rangle + \cos 2\alpha_6 \cos 2\alpha_7\|1\rangle)\|\mathrm{up}_2\rangle$

2.2.2. *Evolution under different parameters $D = -0.655$ and $D = -2$*

In order to enhance our understanding and research on the Hermitian Hamiltonian, we have added other parameters of D. H_1 and H_2 correspond to the Hamiltonians for $D = -0.655$ and $D = -2$, respectively, with their experimental setups illustrated in Fig. S5. These implementations employ the same decomposition method as the $D = 0$ case, but require more complex sequences of optical operations.

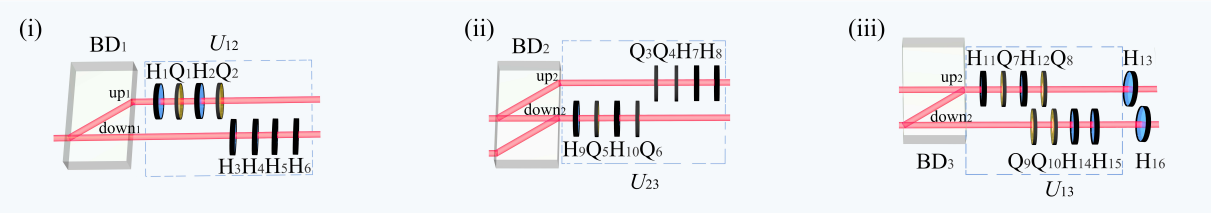

Figure S5. Experimental setup of $D = -0.655$ and $D = -2$. The simulation of temporal dynamics is achieved through precise adjustments of HWPs and QWPs angles within each U_{ij} subunit, with complete experimental parameters provided in Table. II.

Based on the Eq. (S25), the Hamiltonian H_1 with $D = -0.655$ can be expressed as

$$H_1 = \begin{pmatrix} -1.31 & -2 & 0 \\ -2 & -2.62 & -\sqrt{3} \\ 0 & -\sqrt{3} & -3.93 \end{pmatrix}. \tag{S35}$$

Since its evolved form is $U_1 = e^{-iH_1 t}$, its matrix representation can be formulated as

$$\begin{aligned} U_1 = {} & ((0.54\cos 0.405t + 0.367\cos 2.771t + 0.093\cos 5.494t) + i(-0.54\sin 0.405t + 0.367\sin 2.771t + 0.093\sin 5.494t))|1\rangle\langle 1| \\ & + ((-0.463\cos 0.405t + 0.268\cos 2.771t + 0.195\cos 5.494t) + i(0.463\sin 0.405t + 0.268\sin 2.771t + 0.195\sin 5.494t))|1\rangle\langle 2| \\ & + ((0.185\cos 0.405t - 0.401\cos 2.771t + 0.216\cos 5.494t) + i(-0.185\sin 0.405t - 0.401\sin 2.771t + 0.216\sin 5.494t))|1\rangle\langle 3| \\ & + ((-0.463\cos 0.405t + 0.268\cos 2.771t + 0.195\cos 5.494t) + i(0.463\sin 0.405t + 0.268\sin 2.771t + 0.195\sin 5.494t))|2\rangle\langle 1| \\ & + ((0.397\cos 0.405t + 0.196\cos 2.771t + 0.407\cos 5.494t) + i(-0.397\sin 0.405t + 0.196\sin 2.771t + 0.407\sin 5.494t))|2\rangle\langle 2| \\ & + ((-0.159\cos 0.405t - 0.293\cos 2.771t + 0.451\cos 5.494t) + i(0.159\sin 0.405t - 0.293\sin 2.771t + 0.451\sin 5.494t))|2\rangle\langle 3| \\ & + ((0.185\cos 0.405t - 0.401\cos 2.771t + 0.216\cos 5.494t) + i(-0.185\sin 0.405t - 0.401\sin 2.771t + 0.216\sin 5.494t))|3\rangle\langle 1| \\ & + ((-0.159\cos 0.405t - 0.293\cos 2.771t + 0.451\cos 5.494t) + i(0.159\sin 0.405t - 0.293\sin 2.771t + 0.451\sin 5.494t))|3\rangle\langle 2| \\ & + ((0.063\cos 0.405t + 0.437\cos 2.771t + 0.5\cos 5.494t) + i(-0.063\sin 0.405t + 0.437\sin 2.771t + 0.5\sin 5.494t))|3\rangle\langle 3|. \end{aligned} \tag{S36}$$

The evolution process of H_1 (or H_2) under a fixed initial state $|\psi_0\rangle$ is detailed in Table. II. The outcomes are obtained byrotating the angles of the HWP and the QWP.

TABLE II. The preparation of the unitary operators U_1 (or U_2) in the case of $D = -0.655$ (or $D = -2$).

State prepared	Result
H_0 ($\alpha_0 = 0°$)	$\|0\rangle$
BD_1	$\|0\rangle\|down_1\rangle$
H_{3-5} ($\alpha_{3-5} = 0°$)	$\|0\rangle\|down_1\rangle$
H_6 ($\alpha_6 = 45°$)	$\|1\rangle\|down_1\rangle$
BD_2	$\|1\rangle\|dowm_2\rangle$
H_9 (α_9)	$\sin 2\alpha_9\|0\rangle\|down_2\rangle - \cos 2\alpha_9\|1\rangle\|down_2\rangle$
Q_5 (β_9)	$\frac{1+i}{2}(\sin 2\alpha_9 - i\sin 2(\alpha_9-\beta_5))\|0\rangle\|down_2\rangle + \frac{1-i}{2}(-i\cos 2\alpha_9 + \cos 2(\alpha_9-\beta_5))\|1\rangle\|down_2\rangle$
H_{10} (α_{10})	$\frac{-1-i}{2}(\sin 2(\alpha_{10}-\alpha_9)+i\sin 2(\alpha_{10}+\alpha_9-\beta_5))\|0\rangle\|down_2\rangle+\frac{1+i}{2}(\cos 2(\alpha_{10}-\alpha_9)+ i\cos 2(\alpha_{10}+\alpha_9-\beta_5))\|1\rangle\|down_2\rangle$
Q_6 (β_6)	$(-i\cos(2\alpha_9-\beta_5-\beta_6)\sin(2\alpha_{10}-\beta_5-\beta_6)+\cos(2\alpha_{10}-\beta_5-\beta_6)\sin(2\alpha_9-\beta_5-\beta_6))\|0\rangle\|down_2\rangle + (\frac{i}{2}(\cos 2(\alpha_{10}-\alpha_9) + i(\cos 2(\alpha_{10}+\alpha_9-\beta_5) + \cos 2(\alpha_{10}-\alpha_9-\beta_6)+i\cos 2(\alpha_{10}+\alpha_9-\beta_5-\beta_6))))\|1\rangle\|down_2\rangle$
BD_3	$(-i\cos(2\alpha_9-\beta_5-\beta_6)\sin(2\alpha_{10}-\beta_5-\beta_6)+\cos(2\alpha_{10}-\beta_5-\beta_6)\sin(2\alpha_9-\beta_5-\beta_6))\|0\rangle\|down_2\rangle + (\frac{i}{2}(\cos 2(\alpha_{10}-\alpha_9) + i(\cos 2(\alpha_{10}+\alpha_9-\beta_5) + \cos 2(\alpha_{10}-\alpha_9-\beta_6)+i\cos 2(\alpha_{10}+\alpha_9-\beta_5-\beta_6))))\|1\rangle\|up_2\rangle$
H_{11} (α_{11})	$(-i\cos(2\alpha_9-\beta_5-\beta_6)\sin(2\alpha_{10}-\beta_5-\beta_6)+\cos(2\alpha_{10}-\beta_5-\beta_6)\sin(2\alpha_9-\beta_5-\beta_6))\sin 2\alpha_{11}\|0\rangle\|down_2\rangle + \frac{1}{2}\cos 2\alpha_{11}(-i\cos 2(\alpha_{10}-\alpha_9) + \cos 2(\alpha_{10}+\alpha_9-\beta_5) + \cos 2(\alpha_{10}-\alpha_9-\beta_6) + i\cos 2(\alpha_{10}+\alpha_9-\beta_5-\beta_6))\|1\rangle\|up_2\rangle + \frac{i}{2}(\cos 2(\alpha_{10}-\alpha_9) + i(\cos 2(\alpha_{10}+\alpha_9-\beta_5) + \cos 2(\alpha_{10}-\alpha_9-\beta_6) + i\cos 2(\alpha_{10}+\alpha_9-\beta_5-\beta_6)))\|0\rangle\|up_2\rangle$
Q_7 (β_7)	$(-i\cos(2\alpha_9-\beta_5-\beta_6)\sin(2\alpha_{10}-\beta_5-\beta_6)+\cos(2\alpha_{10}-\beta_5-\beta_6)\sin(2\alpha_9-\beta_5-\beta_6))\sin 2\alpha_{11}\|0\rangle\|down_2\rangle + \frac{1+i}{4}(-i\cos 2(\alpha_{10}-\alpha_9) + \cos 2(\alpha_{10}+\alpha_9-\beta_5) + \cos 2(\alpha_{10}-\alpha_9-\beta_6) + i\cos 2(\alpha_{10}+\alpha_9-\beta_5-\beta_6))(\cos 2\alpha_{11} + i\cos 2(\alpha_{11}-\beta_7))\|1\rangle\|up_2\rangle + \frac{1+i}{4}(\cos 2(\alpha_{10}-\alpha_9) + i(\cos 2(\alpha_{10}+\alpha_9-\beta_5) + \cos 2(\alpha_{10}-\alpha_9-\beta_6) + i\cos 2(\alpha_{10}+\alpha_9-\beta_5-\beta_6)))(i\sin 2\alpha_{11} + \sin 2(\alpha_{11}-\beta_7))\|0\rangle\|up_2\rangle$
H_{12} (α_{12})	$(-i\cos(2\alpha_9-\beta_5-\beta_6)\sin(2\alpha_{10}-\beta_5-\beta_6)+\cos(2\alpha_{10}-\beta_5-\beta_6)\sin(2\alpha_9-\beta_5-\beta_6))\sin 2\alpha_{11}\|0\rangle\|down_2\rangle + \frac{-1+i}{4}(\cos 2(\alpha_{10}-\alpha_9) + i\cos 2(\alpha_{10}+\alpha_9-\beta_5) + \cos 2(\alpha_{10}-\alpha_9-\beta_6) + i\cos 2(\alpha_{10}+\alpha_9-\beta_5-\beta_6))(\cos 2(\alpha_{11}-\alpha_{12}) + i\cos 2(\alpha_{11}+\alpha_{12}-\beta_7))\|1\rangle\|up_2\rangle+\frac{1+i}{4}(\cos 2(\alpha_{10}-\alpha_9)+i(\cos 2(\alpha_{10}+\alpha_9-\beta_5)+ \cos 2(\alpha_{10}-\alpha_9-\beta_6) + i\cos 2(\alpha_{10}+\alpha_9-\beta_5-\beta_6)))(i\sin 2\alpha_{11}-\alpha_{12} + \sin 2(\alpha_{11}+\alpha_{12}-\beta_7))\|0\rangle\|up_2\rangle$
Q_8 (β_8)	$(-i\cos(2\alpha_9-\beta_5-\beta_6)\sin(2\alpha_{10}-\beta_5-\beta_6)+\cos(2\alpha_{10}-\beta_5-\beta_6)\sin(2\alpha_9-\beta_5-\beta_6))\sin 2\alpha_{11}\|0\rangle\|down_2\rangle+\frac{-1}{4}(\cos 2(\alpha_{10}-\alpha_9)+i\cos 2(\alpha_{10}+\alpha_9-\beta_5)+\cos 2(\alpha_{10}-\alpha_9-\beta_6)+i\cos 2(\alpha_{10}+\alpha_9-\beta_5-\beta_6))(\cos 2(\alpha_{11}-\alpha_{12})+i\cos 2(\alpha_{11}+\alpha_{12}-\beta_7)+ i\cos 2(\alpha_{11}+\alpha_{12}-\beta_7-\beta_8)\cos 2(\alpha_{11}\alpha_{12}+\beta_8))\|1\rangle\|up_2\rangle +$ $\frac{-1}{4}(\cos 2(\alpha_{10}-\alpha_9) + i(\cos 2(\alpha_{10}+\alpha_9-\beta_5) + \cos 2(\alpha_{10}-\alpha_9-\beta_6) + i\cos 2(\alpha_{10}+\alpha_9-\beta_5-\beta_6)))(\sin 2(\alpha_{11}-\alpha_{12}) - i\sin 2(\alpha_{11}+\alpha_{12}-\beta_7) - i\sin 2(\alpha_{11}+\alpha_{12}-\beta_7-\beta_8)+\sin 2(\alpha_{11}-\alpha_{12}\beta_8))\|0\rangle\|up_2\rangle$
Q_{9-10} ($\beta_{9-10} = 0°$)	$(-i\cos(2\alpha_9-\beta_5-\beta_6)\sin(2\alpha_{10}-\beta_5-\beta_6)+\cos(2\alpha_{10}-\beta_5-\beta_6)\sin(2\alpha_9-\beta_5-\beta_6))\sin 2\alpha_{11}\|0\rangle\|down_2\rangle+\frac{-1}{4}(\cos 2(\alpha_{10}-\alpha_9)+i\cos 2(\alpha_{10}+\alpha_9-\beta_5)+\cos 2(\alpha_{10}-\alpha_9-\beta_6)+i\cos 2(\alpha_{10}+\alpha_9-\beta_5-\beta_6))(\cos 2(\alpha_{11}-\alpha_{12})+i\cos 2(\alpha_{11}+\alpha_{12}-\beta_7)+ i\cos 2(\alpha_{11}+\alpha_{12}-\beta_7-\beta_8)\cos 2(\alpha_{11}\alpha_{12}+\beta_8))\|1\rangle\|up_2\rangle +$ $\frac{-1}{4}(\cos 2(\alpha_{10}-\alpha_9) + i(\cos 2(\alpha_{10}+\alpha_9-\beta_5) + \cos 2(\alpha_{10}-\alpha_9-\beta_6) + i\cos 2(\alpha_{10}+\alpha_9-\beta_5-\beta_6)))(\sin 2(\alpha_{11}-\alpha_{12}) - i\sin 2(\alpha_{11}+\alpha_{12}-\beta_7) - i\sin 2(\alpha_{11}+\alpha_{12}-\beta_7-\beta_8)+\sin 2(\alpha_{11}-\alpha_{12}\beta_8))\|0\rangle\|up_2\rangle$
H_{14-15} ($\alpha_{14-15} = 0°$)	$(-i\cos(2\alpha_9-\beta_5-\beta_6)\sin(2\alpha_{10}-\beta_5-\beta_6)+\cos(2\alpha_{10}-\beta_5-\beta_6)\sin(2\alpha_9-\beta_5-\beta_6))\sin 2\alpha_{11}\|0\rangle\|down_2\rangle+\frac{-1}{4}(\cos 2(\alpha_{10}-\alpha_9)+i\cos 2(\alpha_{10}+\alpha_9-\beta_5)+\cos 2(\alpha_{10}-\alpha_9-\beta_6)+i\cos 2(\alpha_{10}+\alpha_9-\beta_5-\beta_6))(\cos 2(\alpha_{11}-\alpha_{12})+i\cos 2(\alpha_{11}+\alpha_{12}-\beta_7)+ i\cos 2(\alpha_{11}+\alpha_{12}-\beta_7-\beta_8)\cos 2(\alpha_{11}\alpha_{12}+\beta_8))\|1\rangle\|up_2\rangle +$ $\frac{-1}{4}(\cos 2(\alpha_{10}-\alpha_9) + i(\cos 2(\alpha_{10}+\alpha_9-\beta_5) + \cos 2(\alpha_{10}-\alpha_9-\beta_6) + i\cos 2(\alpha_{10}+\alpha_9-\beta_5-\beta_6)))(\sin 2(\alpha_{11}-\alpha_{12}) - i\sin 2(\alpha_{11}+\alpha_{12}-\beta_7) - i\sin 2(\alpha_{11}+\alpha_{12}-\beta_7-\beta_8)+\sin 2(\alpha_{11}-\alpha_{12}\beta_8))\|0\rangle\|up_2\rangle$

Here, the choice of H_1 results in the form of U_1 not being expressible as the elegant analytical solution shown in Eq. (S31). Consequently, the U_{ij} decomposed according to U_1 also fails to provide an analytical solution form. However, we list the corresponding matrices for U_{ij} at $t = 0.4$ as an example:

$$U_{12} = \begin{pmatrix} -0.163 + 0.587i & -0.663 - 0.434i & 0 \\ -0.664 + 0.433i & 0.161 + 0.588i & 0 \\ 0 & 0 & 1 \end{pmatrix}, \tag{S37}$$

$$U_{23} = \begin{pmatrix} 1 & 0 & 0 \\ 0 & 0.802 - 0.188i & -0.552 + 0.129i \\ 0 & 0.552 + 0.129i & 0.802 + 0.188i \end{pmatrix}, \tag{S38}$$

$$U_{13} = \begin{pmatrix} 0.176 - 0.938i & 0 & -0.204 - 0.218i \\ 0 & 1 & 0 \\ 0.204 - 0.218i & 0 & 0.176 + 0.938i \end{pmatrix}. \tag{S39}$$

Similar to the process for handling H_1, we first express H_2 as

$$H_2 = \begin{pmatrix} -4 & -2 & 0 \\ -2 & -8 & -\sqrt{3} \\ 0 & -\sqrt{3} & -12 \end{pmatrix}, \tag{S40}$$

and accordingly, the corresponding unitary operation $U_2 = e^{-iH_2t}$ is represented as

$$\begin{aligned} U_2 = {} & ((0.832\cos 3.119t + 0.16\cos 8.174t + 0.007\cos 12.706t) + i(0.832\sin 3.119t + 0.16\sin 8.174t + 0.007\sin 12.706t))|1\rangle\langle 1| \\ & + ((-0.367\cos 3.119t + 0.334\cos 8.174t + 0.033\cos 12.706t) + i(-0.367\sin 3.119t + 0.334\sin 8.174t + 0.033\sin 12.706t))|1\rangle\langle 2| \\ & + ((0.071\cos 3.119t - 0.151\cos 8.174t + 0.08\cos 12.706t) + i(0.071\sin 3.119t - 0.151\sin 8.174t + 0.08\sin 12.706t))|1\rangle\langle 3| \\ & + ((-0.367\cos 3.119t + 0.334\cos 8.174t + 0.033\cos 12.706t) + i(-0.367\sin 3.119t + 0.334\sin 8.174t + 0.033\sin 12.706t))|2\rangle\langle 1| \\ & + ((0.161\cos 3.119t + 0.697\cos 8.174t + 0.142\cos 12.706t) + i(0.161\sin 3.119t + 0.697\sin 8.174t + 0.142\sin 12.706t))|2\rangle\langle 2| \\ & + ((-0.031\cos 3.119t - 0.316\cos 8.174t + 0.347\sin 12.706t) + i(-0.031\sin 3.119t - 0.316\sin 8.174t + 0.347\sin 12.706t))|2\rangle\langle 3| \\ & + ((0.071\cos 3.119t - 0.151\cos 8.174t + 0.08\cos 12.706t) + i(0.071\sin 3.119t - 0.151\sin 8.174t + 0.08\sin 12.706t))|3\rangle\langle 1| \\ & + ((-0.031\cos 3.119t - 0.316\cos 8.174t + 0.347\sin 12.706t) + i(-0.031\sin 3.119t - 0.316\sin 8.174t + 0.347\sin 12.706t))|3\rangle\langle 2| \\ & + ((0.006\cos 3.119t + 0.143\cos 8.174t + 0.851\cos 12.706t) + i(0.006\sin 3.119t + 0.143\sin 8.174t + 0.851\sin 12.706t))|3\rangle\langle 3|. \end{aligned} \tag{S41}$$

With $t = 0.4$ as an example, the form of U_{ij} resulting from the decomposition of U_2 is

illustrated as

$$U_{12} = \begin{pmatrix} 0.037 + 0.699i & -0.463 - 0.544i & 0 \\ -0.551 + 0.455i & -0.158 + 0.681i & 0 \\ 0 & 0 & 1 \end{pmatrix}, \tag{S42}$$

$$U_{23} = \begin{pmatrix} 1 & 0 & 0 \\ 0 & 0.096 + 0.842i & 0.429 - 0.313i \\ 0 & -0.429 - 0.313094i & 0.096 - 0.842i \end{pmatrix}, \tag{S43}$$

$$U_{13} = \begin{pmatrix} 0.967 - 0.09i & 0 & 0.0118 + 0.238i \\ 0 & 1 & 0 \\ -0.0118 = +0.238i & 0 & 0.967 + 0.09i \end{pmatrix}. \tag{S44}$$

2.3. Evolution method for non-Hermitian Hamiltonian $D = 0$

In this experiment, we have realized the non-Hermitian Hamiltonian $H = H_{\mathrm{dPXP}}^{(-\pi)}$, the expression of which is presented in Eq. (S27). In the context of a 3D space, we have employed a method based on singular value decomposition (SVD) $\mathbb{U} = e^{-iH_{D=0}^{-\pi}t} = USV$ [8]. U (V) is unitary operator, and S as a diagonal operation with non-negative entries, and then decompose it into a product of a series of 2D unitary matrices. The experimental setup of the evolution method for Hermitian model is shown in Fig. S6.

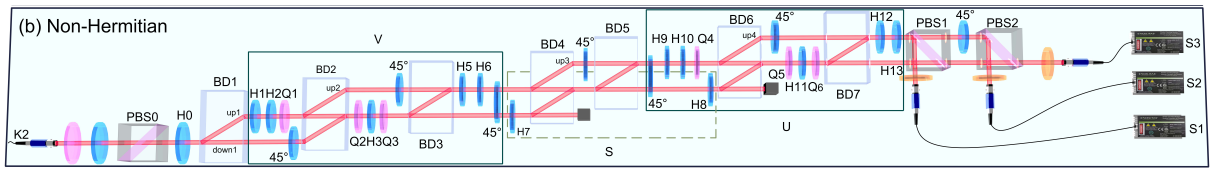

Figure S6. Experimental setup of the non-Hermitian model. The implementation of the non-Hermitian evolution operator follows a distinct decomposition strategy from the Hermitian case. The overall operator is first subjected to a singular value decomposition (SVD). Subsequently, each component resulting from the SVD is further decomposed into a sequence of 2×2 unitary operators. We use PBS_0, H_1 and BD_1 to encode the polarization information of the signal photons entering at port K_2 and to prepare the required initial state. These unitary operations are physically realized via path encoding using the depicted optical elements, including waveplates (H_{1-13} and Q_{1-6}) and BD_{1-7}.

U and V are unitary operators, and S as a diagonal operator with non-negative entries. The unitary operator V_{ij} $(i,j=1,2,3.\ i\neq j)$ is implemented with H_{1-6} and Q_{1-3} after BD_1.The diagonal operator S is put into action through $\mathrm{H}_{7,8}$ and BD_{4-6}. The unitary operator U_{ij} is realized with H_{9-13} and Q_{4-6} after BD_5. $\mathrm{H}_{13,16}$ and BD_7 are used for the final interference. The final state evolved after these unitary operations is measured by a measurement module composed of PBS_1, a HWP (45°) and PBS_2. After passing through the measurement module, the photons are collected by S_{1-3} through FP, and the idle photons collected by another SPD are counted together. The initial state prepared in the experiment as $|\psi_3(\pi)\rangle=(|\mathbb{Z}_2\rangle-|\mathbb{Z}_2'\rangle)/\sqrt{2}=|3\rangle$ with $L=6$, where $|3\rangle:=|\mathrm{H}\rangle|\mathrm{down}_1\rangle$.

According to the Eq. (S27), the non-Hermitian Hamiltonian H_3 with $D=0$ can be expressed as

$$H_3=\begin{pmatrix}0 & -2(1-g) & 0\\ -2(1+g) & 0 & -\sqrt{3}(1-g)\\ 0 & -\sqrt{3}(1+g) & 0\end{pmatrix}. \tag{S45}$$

Since its evolved form is $\mathbb{U}=e^{-iH_3t}$, its matrix representation can be formulated as

$$\mathbb{U}=\begin{pmatrix}\frac{1}{7}(3+4\cosh[\sqrt{7}\sqrt{-1+g^2}t]) & -\frac{2i(-1+g)\sinh[\sqrt{7}\sqrt{-1+g^2}t]}{\sqrt{7}\sqrt{-1+g^2}} & -\frac{2\sqrt{3}(-1+g)(-1+\cosh[\sqrt{7}\sqrt{-1+g^2}t])}{7(1+g)}\\ \frac{2i(1+g)\sinh[\sqrt{7}\sqrt{-1+g^2}t]}{\sqrt{7}\sqrt{-1+g^2}} & \cosh[\sqrt{7}\sqrt{-1+g^2}t] & -i\frac{\sqrt{\frac{3}{7}}(-1+g)\sinh[\sqrt{7}\sqrt{-1+g^2}t]}{\sqrt{-1+g^2}}\\ -\frac{2\sqrt{3}(1+g)(-1+\cosh[\sqrt{7}\sqrt{-1+g^2}t])}{7(1+g)} & i\frac{\sqrt{\frac{3}{7}}(1+g)\sinh[\sqrt{7}\sqrt{-1+g^2}t]}{\sqrt{-1+g^2}} & \frac{1}{7}(3+4\cosh[\sqrt{7}\sqrt{-1+g^2}t])\end{pmatrix}. \tag{S46}$$

Given the complexity of the analytical SVD of $\mathbb{U}$, we consider a specific example with $g=0.2$ $(t=0.4)$ to present the corresponding numerical results. First, we provide the decomposition of the unitary operater V,

$$V=\begin{pmatrix}0.7853139411543668 & -0.5672020334732046 & -0.24812067034500962\\ 0.5674940565426148\mathrm{i} & 0.4993238670332199\mathrm{i} & 0.6546954800514503\mathrm{i}\\ -0.2474520349833533 & -0.6549484934213169 & 0.7140097767872257\end{pmatrix}. \tag{S47}$$

The unitary operators V_{ij} as

$$V_{12}=\begin{pmatrix}0.6605750303252698 & -0.7507600344389468 & 0\\ 0.7507600344389467\mathrm{i} & 0.6605750303252698\mathrm{i} & 0\\ 0 & 0 & 1\end{pmatrix}, \tag{S48}$$

$$V_{23} = \begin{pmatrix} 1 & 0 & 0 \\ 0 & 0.7558927360414313 & 0.6546954800514504\mathrm{i} \\ 0 & 0.6546954800514504\mathrm{i} & 0.7558927360414313 \end{pmatrix}, \tag{S49}$$

$$V_{13} = \begin{pmatrix} 0.9445913986770871 & 0 & -0.3282485179635459 \\ 0 & 1 & 0 \\ 0.3282485179635459 & 0 & 0.9445913986770871 \end{pmatrix}. \tag{S50}$$

Then, The operator S corresponds to a diagonal matrix,

$$S = \begin{pmatrix} 1 & 0 & 0 \\ 0 & 0.818 & 0 \\ 0 & 0 & 0.668 \end{pmatrix}. \tag{S51}$$

And another unitary operater U as,

$$U = \begin{pmatrix} 0.24812067034501029 & -0.5672020334732053 & -0.24812067034500962 \\ 0.6546954800514512\mathrm{i} & -0.4993238670332173\mathrm{i} & 0.5674940565426155\mathrm{i} \\ -0.7140097767872242 & -0.6549484934213176 & 0.24745203498335488 \end{pmatrix}, \tag{S52}$$

$$U_{12} = \begin{pmatrix} -0.6064337091410452 & -0.7951340493384955 & 0 \\ 0.7951340493384955\mathrm{i} & -0.6064337091410452\mathrm{i} & 0 \\ 0 & 0 & 1 \end{pmatrix}, \tag{S53}$$

$$U_{23} = \begin{pmatrix} 1 & 0 & 0 \\ 0 & 0.8233774928845254 & 0.5674940565426156\mathrm{i} \\ 0 & 0.5674940565426156\mathrm{i} & 0.8233774928845254 \end{pmatrix}, \tag{S54}$$

$$U_{13} = \begin{pmatrix} 0.30053291123669174 & 0 & -0.9537714449822865 \\ 0 & 1 & 0 \\ 0.9537714449822865 & 0 & 0.30053291123669174 \end{pmatrix}. \tag{S55}$$

3. THE RESULT OF THE EXPERIMENT

3.1. The experimental result for Hermitian case

We list the experimental results for the fidelity of $D = 0, -0.655, -2$ in the Hermitian case, as shown in Table. III

TABLE III. The fidelity of D for different times.

t	$D = 0$ ($\pm 10^{-5}$)	$D = -0.655$ ($\pm 10^{-5}$)	$D = -2$ ($\pm 10^{-5}$)
0	0.99790(1325)	0.99882(229)	0.99692(268)
0.4	0.59478(1029)	0.61480(159)	0.68047(223)
0.8	0.10871(333)	0.14875(98)	0.52973(197)
1.2	0.00801(88)	0.01524(50)	0.91767(255)
1.6	0.11496(371)	0.25247(118)	0.86026(234)
2	0.64928(1095)	0.83958(193)	0.52886(183)
2.4	0.99464(1396)	0.87237(205)	0.71807(221)
2.8	0.51848(92)	0.45198(148)	0.97627(261)
3.2	0.09305(71)	0.13433(103)	0.66460(193)
3.6	0.01935(38)	0.01649(59)	0.53247(169)
4	0.16361(60)	0.46289(148)	0.93279(231)
4.4	0.70006(87)	0.87166(198)	0.84523(230)
4.8	0.98660(118)	0.72326(178)	0.50632(167)
5.2	0.52759(126)	0.44003(132)	0.75521(193)
5.6	0.09074(70)	0.06154(100)	0.96239(191)
6	0.02184(38)	0.10460(84)	0.64102(205)
6.4	0.18050(59)	0.53415(126)	0.55709(176)
6.8	0.73005(98)	0.75631(166)	0.93240(185)
7.2	0.96925(124)	0.73345(182)	0.83688(213)
7.6	0.49047(132)	0.39389(159)	0.49370(188)
8	0.07810(71)	0.00756(75)	0.77497(181)

3.2. The experimental result for non-Hermitian case

We list the experimental results for the fidelity of $g = 0.2, 0.9, 1, 1.1$ in the non-Hermitian case, as shown in Table. IV.

TABLE IV. The fidelity of g for different times.

t	$g = 0.2$ ($\pm 10^{-5}$)	$g = 0.9$ ($\pm 10^{-5}$)	$g = 1$ ($\pm 10^{-5}$)	$g = 1.1$ ($\pm 10^{-5}$)
0	0.99987(10)	0.99990(13)	0.99987(9)	0.99988(8)
0.4	0.72779(374)	0.99607(92)	0.99999(9)	0.99647(77)
0.8	0.22104(638)	0.98074(202)	0.99415(11)	0.98366(162)
1.2	0.04734(323)	0.94534(443)	0.99805(7)	0.96567(216)
1.6	0.20523(608)	0.89980(796)	0.99953(7)	0.94304(302)
2	0.69166(562)	0.83643(1495)	0.99795(8)	0.92656(329)
2.4	0.99908(33)	0.83945(2407)	1.00026(6)	0.92042(356)
2.8	0.75218(511)	0.89062(2961)	0.99546(8)	0.91030(370)
3.2	0.24598(613)	0.82747(2082)	0.99292(14)	0.90826(379)
3.6	0.05167(361)	0.86596(1158)	0.99827(17)	0.90317(350)
4	0.18531(607)	0.92328(602)	0.99954(17)	0.90182(365)
4.4	0.65344(544)	0.96607(338)	1.00407(16)	0.89912(390)
4.8	0.99589(66)	0.98716(168)	0.99892(16)	0.90150(391)
5.2	0.77559(471)	0.99805(62)	0.99985(18)	0.89816(358)
5.6	0.27762(612)	0.99972(24)	1.00265(16)	0.89491(386)
6	0.04800(354)	0.99258(119)	1.00002(17)	0.90104(385)
6.4	0.16477(540)	0.97074(292)	1.00061(14)	0.89787(366)
6.8	0.62966(591)	0.92209(605)	0.99773(18)	0.89376(383)
7.2	0.99059(102)	0.89060(953)	0.99911(18)	0.89479(366)
7.6	0.80555(461)	0.85438(1653)	0.99975(17)	0.88915(409)
8	0.30488(653)	0.89221(2677)	1.00063(16)	0.89702(381)

3.3. The experimental result for exceptional point

In the non-Hermitian case, we have calculated the eigenvalues of H_3 as follows

$$E_1 = 0,\ E_2 = \sqrt{7}\sqrt{1-g^2},\ E_3 = -\sqrt{7}\sqrt{1-g^2}. \tag{S56}$$

We list the experimental results corresponding to the real and imaginary parts(S56) of different g ($t = 0.4$) in the non-Hermitian case, as shown in Table. V.

TABLE V. The results of $t = 0.4$ for different g.

g	Experimental vale g ($\pm 10^{-5}$)	$\mathrm{Rm}_{\pm}$ ($\pm 10^{-5}$)	Theoretical value($\pm$)	$\mathrm{Im}_{\pm}$ ($\pm 10^{-5}$)	Theoretical value($\pm$)
0	0.00901(1438)	2.64564(48)	2.64575	0	0
0.2	0.19544(1472)	2.59473(775)	2.59230	0	0
0.4	0.40455(1208)	2.41958(1416)	2.42487	0	0
0.6	0.59930(1095)	2.11800(2167)	2.11660	0	0
0.8	0.79924(1114)	1.59012(3929)	1.58745	0	0
0.9	0.90158(1124)	1.14461(6265)	1.15326	0	0
1	0.98408(1440)	0.47021(30523)	0	0	0
1.1	1.08391(1295)	0	0	1.10637(9004)	1.21244
1.2	1.19716(1187)	0	0	1.74135(5720)	1.75499
1.4	1.39605(1368)	0	0	2.57733(5189)	2.59230
1.6	1.59381(1469)	0	0	3.28354(4991)	3.30454
1.8	1.79274(1752)	0	0	3.93674(5584)	3.95980
2	2.00104(2204)	0	0	4.58576(6731)	4.58258

[1] James D F V, Kwiat P G, Munro W J, White A G. Measurement of qubits. Phys. Rev. A. **64**, 052312 (2001).

[2] Zhao X, Yu X, Zhou W, Zhang C, Xu J-S, Li C-F, and Guo G-C. Experimental Investigation of Uncertainty Relations for Non-Hermitian Operators. Phys. Rev. Lett. **132**, 070203 (2024).

[3] Yu X, Zhao X, Li L, Hu X-M, Duan X, Yuan H, Zhang C. Toward Heisenberg scaling in non-Hermitian metrology at the quantum regime. Sci. Adv. **10**, eadk7616 (2024).

[4] Kaneda F, Garay-Palmett K, U′Ren A B, and Kwiat P. G. Heralded single-photon source utilizing highly nondegenerate, spectrally factorable spontaneous parametric downconversion. Opt. Express. **24**, 010733 (2016).

[5] Tanida M, Okamoto R and Takeuchi S. Highly indistinguishable heralded single-photon sources using parametric down conversion. Opt. Express. **20**, 015275 (2012).

[6] Montaut N, Sansoni L, Meyer-Scott E, Ricken R, Quiring V, Herrmann H and Silberhorn, C. High-efficiency plug-and-play source of heralded single photons. Phys. Rev. Applied. **8**, 024021 (2017).

[7] Reck M and Zeilinger A, Experimental realization of any discrete unitary operator, Phys. Rev. Lett. **73**, 58 (1994).

[8] M. A. Nielsen, I. L.Chuang, Quantum computation and quantum information, *Cambridge university press* 2010.